Materials and Design 177 (2019) 107831

Contents lists available at ScienceDirect

Materials and Design

journal homepage: www.elsevier.com/locate/matdes

Synthesis of Ag-ZnO core-shell nanoparticles with enhanced photocatalytic activity through atomic layer deposition

Sejong Seong [a,1], In-Sung Park [a,b,1], Yong Chan Jung [a], Taehoon Lee [a], Seon Yong Kim [a], Ji Soo Park [c], Jae-Hyeon Ko [c], Jinho Ahn [a,b,*]

[a] Division of Materials Science and Engineering, Hanyang University, Seoul 04763, Republic of Korea
[b] Institute of Nano Science and Technology, Hanyang University, Seoul 04763, Republic of Korea
[c] Department of Applied Optics and Physics, Hallym University, Gangwon-do 24252, Republic of Korea

HIGHLIGHTS

- The ALD technology is applied to fabricate Ag-ZnO nanoparticles for photocatalyst.
- Stable ZnO shell layers with wurtzite structure are deposited on Ag core particles.
- Ag-ZnO shows ~2.5 to 4 times enhanced photodegradation compared with pure ZnO.
- SPR effect of Ag increases photocatalytic performance of Ag-ZnO photocatalyst.
- Ultra-thin ZnO shells on Ag cores increase photocatalytic performance in UV-region.

GRAPHICAL ABSTRACT

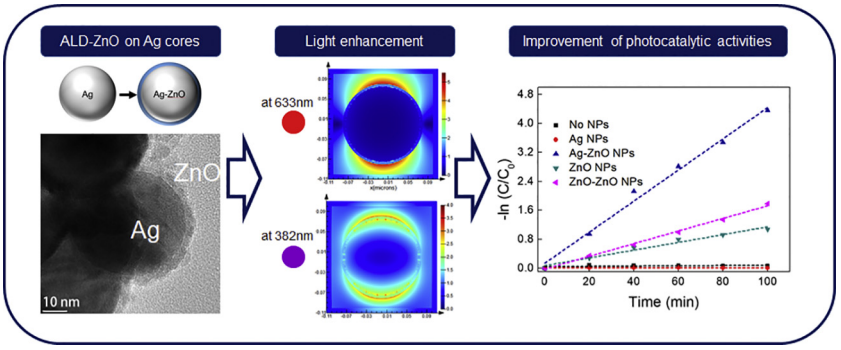

ARTICLE INFO

Article history:
Received 11 February 2019
Received in revised form 25 April 2019
Accepted 5 May 2019
Available online 7 May 2019

Keywords:
Photocatalyst
Core-shell
Surface plasmon resonance
Silver
Zinc oxide
Atomic layer deposition

ABSTRACT

Herein, Ag-ZnO core-shell nanoparticles (NPs) with enhanced photocatalytic activity were prepared by coating Ag metal cores with ZnO semiconductor shells through atomic layer deposition (ALD). Instrumental analysis revealed that the ultra-thin and conformal nature of the shell allowed the core-shell NPs to simultaneously exploit the photocatalytic properties of ZnO and the plasmonic properties of Ag. In a rhodamine B photodegradation test performed under artificial sunlight, Ag-ZnO core-shell NPs exhibited better photocatalytic performance than other prepared photocatalysts, namely ZnO NPs and ALD-ZnO coated ZnO NPs. The performance enhancement was ascribed to the effect of noble metal-semiconductor heterojunctions, which increased the efficiency of electron-hole separation, i.e., the Ag core effectively captured excited electrons at the ZnO surface, which resulted in the elevated production of hydroxyl radicals from holes remaining at ZnO. A three-dimensional finite-difference time-domain simulation of the Ag-ZnO NPs with variable shell thickness showed that ZnO shells on Ag metal cores increase the intensity of light around NPs, allowing the plasmonic cores to fully utilize incident light.

1. Introduction

Environmental problems associated with toxic chemicals and water pollution have inspired extensive research on the establishment of a

* Corresponding author at: Division of Materials Science and Engineering, Hanyang University, Seoul 04763, Republic of Korea.
E-mail address: jhahn@hanyang.ac.kr (J. Ahn).
[1] Both S. Seong and I.-S. Park contributed equally to this work.

https://doi.org/10.1016/j.matdes.2019.107831

sustainable natural environment and the development of human health care [1]. The above problems can possibly be mitigated through the use of functional photocatalysts that can efficiently harvest solar energy and prevent or alleviate the effects of environmental pollution. Among the wide range of newly developed photocatalysts, core-shell nanoparticles (NPs) have attracted much attention in view of their high biochemical stability and excellent performance [2–4]. In particular, core-shell NPs featuring noble metal-semiconductor heterojunctions are promising materials for the solar light-induced decontamination of water [5].

The shells of core-shell NPs are generally prepared by liquid-phase processes (such as sol-gel techniques), which, however, exhibit many disadvantages. For example, the use of these processes often results in the formation of non-conformal coatings, poor control of shell thickness, and the agglomeration of core materials [6]. Therefore, gas-based methods such as atomic layer deposition (ALD) have been suggested as viable alternatives to fabricate ultra-thin and conformal shell coatings [7,8]. In particular, core-shell photocatalysts fabricated by ALD are expected to exhibit enhanced photocatalytic performance and increased lifetime due to the inhibitory effect of the shell on core oxidation.

ZnO is a unique semiconductor photocatalyst exhibiting a wide band gap, high oxidizing strength, good eco-stability, and excellent photocatalytic performance [1,9]. Moreover, the electrical, optical, and catalytic properties of ZnO can be modulated and optimized by controlling the thickness of nanoscale ZnO layers [10]. Previously, TiO_2 has been actively employed as a photocatalyst because of its chemical stability, nontoxicity, and high reactivity. Today, it is believed that ZnO photocatalysts can be engineered to match the performance of TiO_2 ones, as the former semiconductor features an energy band gap (~3.2 eV) and electron affinity (~4.3 eV) similar to those of the latter. ZnO is also cheaper than TiO_2 and is therefore well suited for application in large-scale photocatalytic water purification [11]. However, the fast recombination of photogenerated electrons and holes at the surfaces of both ZnO and TiO_2 results in low photocatalytic efficiency and inefficient utilization of sunlight [12], leaving much room for performance improvement.

The photocatalytic activity of ZnO can be enhanced through its hybridization with noble metals to prolong the lifetime of photogenerated carriers [13]. Typically, noble metals exhibit localized surface plasmon resonance (LSPR) [14,15], which has a beneficial effect on the photocatalytic performance of ZnO [16], especially in the case of metal-semiconductor heterostructures such as mesoporous Ag-ZnO nanocomposites [16] and rod-like Au-ZnO nanocomposites [17]. Ag is commonly employed in LSPR-based composite materials because of its anti-bacterial properties, low cost, and nontoxicity. Besides, Ag-based nanocomposites typically exhibit admirable optical and photoelectrochemical properties. The LSPR of Ag induces light focusing in the vicinity of Ag-ZnO nanocomposites, giving rise to the so-called light enhancement effect. Compared to bare Ag NPs, Ag-ZnO core-shell NPs with conformally deposited ZnO shells feature significantly increased chemical stability and can therefore maintain their properties for a long time, while bare Ag NPs form Ag_2S or Ag_2O when exposed to aqueous solutions and hence quickly lose their pristine properties [18]. Consequently, to effectively isolate Ag core NPs from the reactants and the surrounding medium, ZnO shell layers should feature superior barrier properties.

Herein, ZnO shell layers were conformally and uniformly deposited on Ag core NPs in an ALD system, where the reaction chamber was rotated to prevent NP agglomeration [3]. The ZnO shell layers are functioned as photocatalytic materials and Ag cores are functioned as materials for light enhancement. The photocatalytic activity of as-fabricated Ag-ZnO core-shell NPs was determined in a rhodamine b (RhB) photodegradation test and compared to those of ZnO NPs and ALD-ZnO coated ZnO (ZnO-ZnO) NPs. The light enhancement effects in the visible region induced by the LSPR of the Ag core were verified by three-dimensional (3D) finite-difference time-domain (FDTD) simulation of Ag-ZnO NPs with variable ZnO shell layer thickness.

2. Experimental

2.1. Fabrication of Ag-ZnO core-shell NPs

The ZnO shell layers were deposited on Ag core NPs by ALD method. Ag core NPs (diameter < 150 nm) were purchased from Sigma-Aldrich, USA (Product No. 4840659) and the Brunauer-Emmett-Teller surface area was measured to be 1.98 m^2/g (Micromeritics Co., 3 Flex, USA). The intensity-weighted mean diameter of Ag core NPs dispersed in water was measured as ~140 nm, which means that they are well dispersed in water (Fig. S1). For the fabrication of ZnO shell layers by ALD, diethylzinc and deionized water were used as the metal precursor and the reactant, respectively. 100-cycle of ALD deposition was processed at 150 °C in a rotational ALD system (CN1 Co., Atomic Shell, Korea).

2.2. Instrumental characterization and photocatalytic activity determination

Transmission electron microscopy (TEM), scanning transmission electron microscopy (STEM), and energy-dispersive X-ray spectroscopy (EDXS) mapping analyses (all with JEOL JEM 2100F, Japan) were conducted to confirm the deposition of ZnO on the Ag core. Powder X-ray diffraction (PXRD; Rigaku SmartLab, Japan) was used to probe the crystal structure of ZnO shells. Photoluminescence (PL) measurements were conducted at room temperature using a micro confocal PL spectrometer (Dongwoo, Optron MonoRa-750i, Korea) equipped with a He—Cd laser as an excitation source. The excitation wavelength was fixed at 325 nm. The absorption spectra of photocatalyst-RhB dispersions were measured using an ultraviolet-visible (UV–vis) spectrometer (Perkin Elmer Lambda Co., 650S, USA). For photocatalytic activity determination, Ag-ZnO NPs (5 mg) were dispersed in aqueous RhB (10^{-5} M, 10 mL). Photocatalytic activity was analyzed by monitoring the characteristic absorption band of RhB at 544 nm [19]. The obtained dispersions were kept in the dark to ensure the establishment of an adsorption equilibrium and then irradiated using a solar simulator equipped with a 450-W xenon arc lamp (Sol3A, Newport Sol3A, USA). To quantify photocatalytic activity, 1-mL samples of the reaction mixture were withdrawn at 20-min intervals and transferred into a quartz cuvette to record absorption spectra in the range of 400–700 nm. Light enhancement effects around Ag-ZnO NPs were investigated by numerical calculations employing the 3D-FDTD simulation method of FDTD Solutions software (Lumerical Solutions, Canada).

3. Results and discussion

Fig. 1 shows TEM/STEM images and the corresponding EDXS maps of Ag-ZnO NPs prepared using 100 ALD cycles, revealing that ZnO shells were conformally coated on Ag cores. The low-magnification TEM image (Fig. S2) confirms the conformality of ZnO coating on Ag NPs. Fig. 1(a) and (b) reveal that ALD-ZnO shells with ~5 nm thickness were conformally coated, even at the edges of the cores. The coated NPs appeared to have rough surface morphology of ZnO shells, which is considered to be island coalescence. ALD-induced growth of thin films can be categorized into three major types, namely substrate-inhibited, substrate-enhanced, and linear growth [20]. In the initial stage of ALD, ZnO layer growth is substrate-inhibited and characterized by slow island growth. After island growth is completed, islands coalesce into layers, and thin films are subsequently grown in a layer-by-layer fashion in the so-called steady regime [20].

If the number of ALD cycles is fewer than 100 cycles, the growth of ZnO on NPs can be observed as randomly scattered islands [3,20]. The 5-nm-thick of ZnO on Ag is thin enough to utilize the light enhancement effects induced by plasmonic effect of Ag, as it will be described later. Fig. 1(c) shows EDXS maps of Ag, Zn, and O for several Ag core NPs and the coated Zn shell layer. Since both the core and the shell were spherical, their signals were expected to have a direction-independent

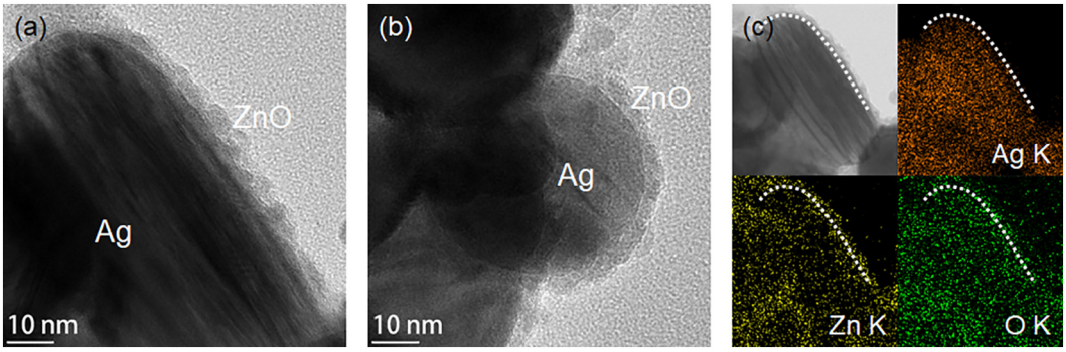

Fig. 1. (a, b) TEM images and (c) STEM image of Ag-ZnO NPs prepared using 100 ALD cycles and the corresponding EDXS maps of Ag, Zn, and O. The white dotted lines show the edge of Ag core.

intensity variation. As can be seen in Fig. 1(c), the signal of Ag K is only detected inside the Ag/ZnO interface. However, the signals of shell-constituting elements (Zn and O) are stronger outside the Ag/ZnO interface, which indicates the full encapsulation of the Ag core by ZnO shell. When typical solution-phase is applied to synthesize ZnO, ZnO tends to grow in the form of nanorods or nanosheets [21,22]. Since ALD technology is a gas-phase method in which reaction occurs only on the surface, ZnO shells grow in the form of thin films, resulting in entire encapsulation of the Ag cores.

Fig. 2 shows the PXRD patterns of Ag and Ag-ZnO NPs along with the standard patterns of Ag and ZnO (JCPDS Nos. 04-0783 and 36-1451, respectively). Since the ZnO-to-Ag proportion was low, the pattern of Ag-ZnO NPs was magnified to identify and characterize ZnO shells. The magnified pattern featured peaks corresponding to reflections from the (100), (002), and (101) planes of pure wurtzite-type ZnO [23]. In particular, the strong and sharp peak of the (002) plane indicated film growth along the *c*-axis, which is related to the hexagonal wurtzite structure of ZnO [24]. The abovementioned wurtzite structure is the most stable phase of ZnO under standard conditions [25], whereas the less stable rocksalt phase is more photocatalytically active because of its narrow band gap (1.8–2.2 eV) and a high capability of absorbing visible light [26]. Unluckily, rocksalt ZnO is very unstable under ambient conditions, and the photocatalytic activity of wurtzite ZnO is therefore commonly enhanced by modifications such as porous structure formation and stabilization under high pressure [26,27]. The results of TEM and PXRD analyses indicated that the employed ALD technique allowed one to conformally obtain ultra-thin layers of wurtzite ZnO and thus fabricate stable metal-semiconductor heterojunction structures. In order for a material to show photocatalytic activity, its irradiation should generate electrons (e^-) and holes (h^+) to subsequently produce superoxide anion radicals and hydroxyl radicals. Herein, we employed PL spectroscopy to obtain direct evidence of electron transfer in Ag-ZnO NPs, demonstrating that the direct contact of ZnO with Ag facilitates the transfer of excited electrons from the conduction band (CB) of ZnO to Ag and induces the separation of e^- and h^+ (i.e., hinders their recombination) to increase photocatalytic activity.

Fig. 3 presents room-temperature PL spectra of Ag and Ag-ZnO NPs, revealing the emergence of a unique UV emission peak upon the coating of Ag core NPs with ZnO. The peak at around 380 nm was ascribed to near-band-edge (~3.25 eV) emission originating from the recombination of e^-–h^+ pairs [1], while the broad visible-range emission of ZnO at 500–700 nm was attributed to deep-level or trap state emission, i.e., to the transfer of electrons from a near-CB shallow donor level to a shallow acceptor level [28]. In addition, the defect level of ZnO was found to lie slightly higher than the Fermi level of Ag, which allowed electrons to flow from the former to the latter. The strong and broad visible emission shown in Fig. 3 should be able to stimulate the SPR of Ag cores and thus enable the transfer of numerous excited electrons of Ag back to the CB of ZnO [17].

Photodegradation of aqueous RhB under simulated sunlight irradiation was chosen as model reaction to examine the photocatalytic activity of Ag-ZnO NPs. The power of the solar simulator was fixed at 1 Sun (120,000 lx) to produce radiation largely within the wavelength region of natural sunlight. The photocatalytic reactions of non-coated Ag,

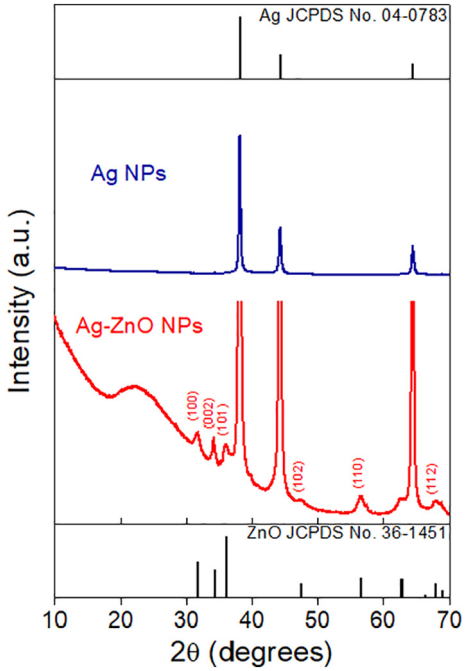

Fig. 2. PXRD patterns of Ag and Ag-ZnO NPs; standard patterns of Ag and ZnO.

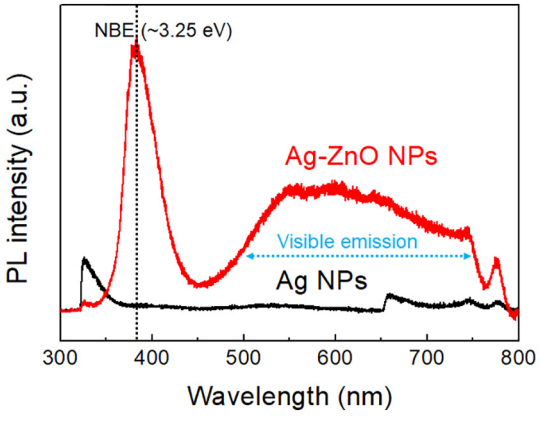

Fig. 3. PL spectra of the Ag and Ag-ZnO NPs recorded at an excitation wavelength of 325 nm.

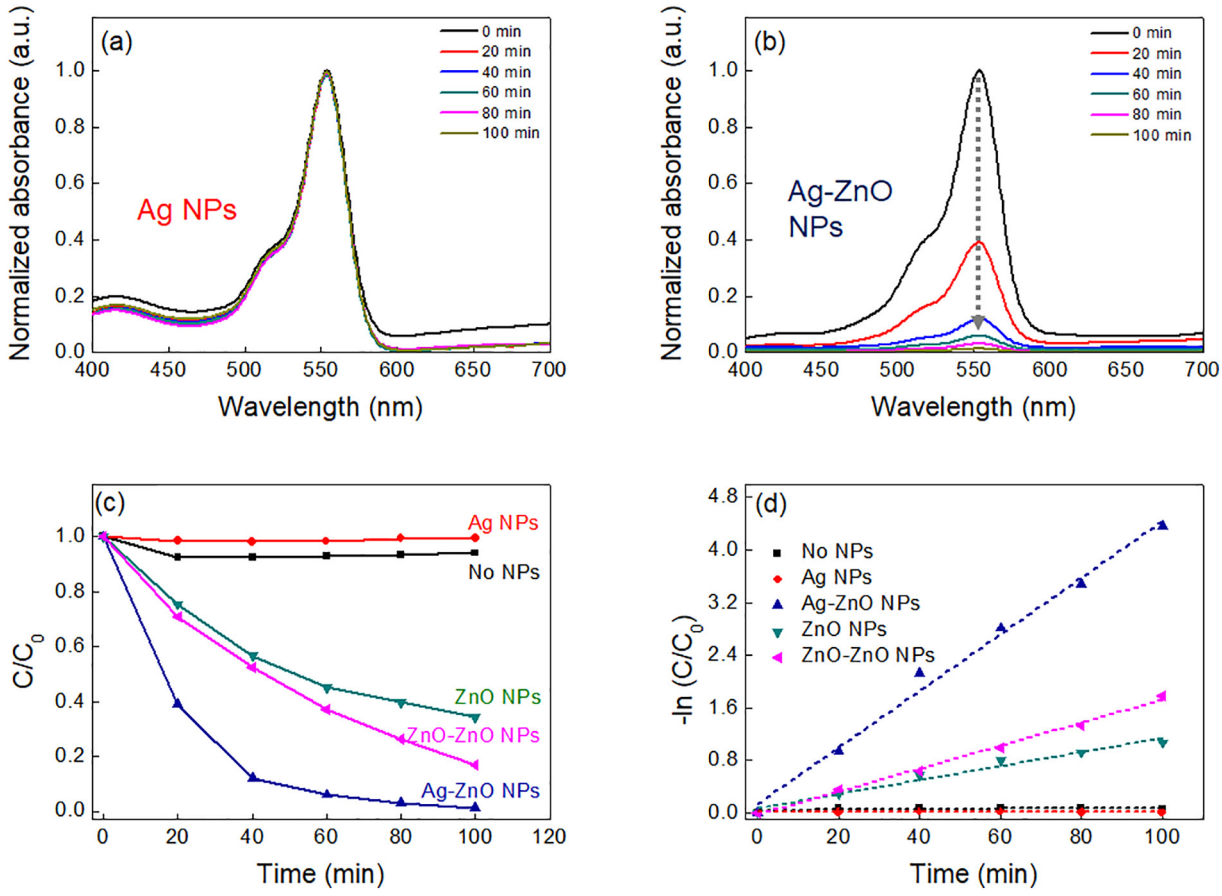

Fig. 4. Normalized absorbance of the RhB solution containing (a) Ag and (b) Ag-ZnO NPs with time of simulated sunlight irradiation. (c, d) Photocatalytic activities of Ag, Ag-ZnO, ZnO, and ZnO-ZnO NPs for RhB degradation; (c) fractions of the initial RhB amount (C/C_0, where C is RhB concentration after irradiation for time t, and C_0 is the initial RhB concentration) remaining in solution after sunlight irradiation; (d) the data in (c) in logarithmic format showing the results of fitting experimental results with a pseudo-first-order kinetic model ($-\ln(C/C_0) = kt$).

purchased ZnO (Product No. 544906, diameter < 100 nm, Sigma-Aldrich, MO, USA), and ALD-ZnO coated ZnO (ZnO-ZnO) NPs were also measured for comparison. The efficiency of photocatalytic RhB degradation was determined based on post-irradiation absorbance at 554 nm [17,19]. Fig. 4(a) and (b) shows the change in absorbance of the RhB solution containing Ag and Ag-ZnO NPs, respectively, with the time of simulated sunlight irradiation. As presented in supplement Fig. S3, photodegradation is observed in the presence of ZnO as expected. However, Ag-ZnO core-shell NPs shows the most enhanced photodegradation performance as compared with ZnO and ZnO-ZnO NPs. Fig. 4(c) shows photocatalytic performances of Ag, Ag-ZnO, ZnO, and ZnO-ZnO NPs for RhB degradation, revealing that no degradation was observed in the absence of catalysts or in the presence of pure Ag NPs. On the other hand, the absorbance of RhB solution decreased with time in the presence of ZnO-containing photocatalysts. In the case of ZnO NPs, ~65% of RhB was degraded after 100-min radiation, while a higher degradation efficiency of 83% was observed for ZnO-ZnO NPs. Notably, the highest degradation efficiency (95% after 60 min) was achieved by Ag-ZnO NPs. There was no change in the crystallographic structure of ZnO shells even after RhB degradation test (Fig. S4). The ZnO shells exhibit stable wurtzite structure observed by the fast Fourier pattern of (100), (002), and (101) planes.

Table 1
Rate constants (k) of solar light irradiation-induced RhB degradation catalyzed by Ag, Ag-ZnO, ZnO, and ZnO-ZnO NPs.

NPs	None	Ag	Ag-ZnO	ZnO	ZnO-ZnO
k (min^{-1})	0.0004	0.0001	0.0430	0.0107	0.0175

Fig. 4(d) presents RhB degradation data as a plot of $-\ln(C/C_0)$ vs. t (where C is RhB concentration after irradiation for time t, and C_0 is the initial RhB concentration) and the corresponding linear fits [29], the slopes of which are taken to equal pseudo-first-order rate constants k (Table 1). As mentioned above, Ag-ZnO NPs showed the highest photocatalytic activity among the tested catalysts, featuring the highest k of 0.0430 min^{-1}, which was ascribed to the increased efficiency of e^-–h^+ separation due to the presence of metal NPs inside ZnO (see Fig. 5). Both the injected electrons from Ag cores and the holes on the ZnO surface were concluded to contribute to the enhancement of photocatalytic activity [12,17].

Fig. 5 shows a schematic diagram of electron transfer in the Ag-ZnO photocatalytic system. Typically, photocatalytic reactions are initiated when the semiconductor absorbs photons with energies higher than that of its band gap. The thus generated electrons are excited from the valence band (VB) to the CB, which creates electrons and holes on the surface of ZnO shells. In general, photogenerated holes in the VB recombine with photoexcited electrons in the CB to generate light. However, oxygen atoms around the photocatalyst can prolong the lifetime of e^-–h^+ pairs, reacting with the photoexcited electrons to produce superoxide radicals, which, in turn, are further converted into highly energetic hydroperoxyl radicals and H_2O_2. Hydroperoxyl radicals also function as electron scavengers, delaying the recombination of e^-–h^+ pairs. At the same time, photogenerated holes react with hydroxide anions in water to afford hydroxyl radicals, an extremely strong and non-selective oxidant, thereby inducing partial or complete mineralization of organics. Moreover, highly reactive holes may also directly oxidize organic matter. In short, the photocatalyst-promoted production of highly reactive hydroxyl radicals and H_2O_2 reduces the rate of e^-–h^+ pair

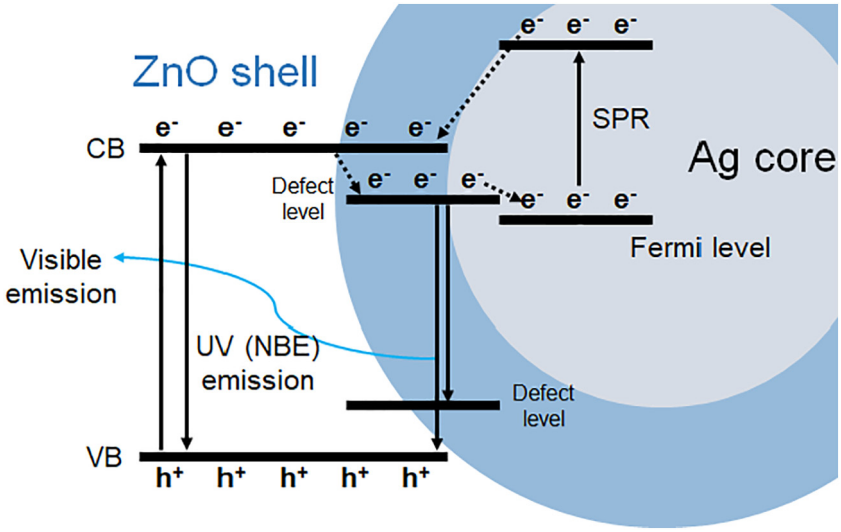

Fig. 5. Schematic diagram of the electrons transfer mechanism of the Ag-ZnO metal-semiconductor heterojunction NPs.

recombination and provides additional time for the reaction of these species with organic pollutant molecules [1,30].

Noble metals such as Ag can act as sinks for photogenerated electrons, promoting interfacial charge transfer between semiconductor shells and noble metal cores [30]. Since the ALD–ZnO layer shows thin thickness and high energy band gap which are enough for visible light to reach the Ag core, ZnO and Ag are photoexcited simultaneously. The excitation of Ag results in electron transfer from Ag to the CB of ZnO, since the surface plasmonic state of the former lies above the CB of the latter. In the same way, irradiation of the ZnO shell promotes electron transfer from the CB of ZnO to the electronic band of Ag, i.e., the metal core captures electrons from the semiconductor and reduces the rate of e^{-}–h^{+} recombination. Additionally, electrons excited by SPR move to the semiconductor CB, which results in the increased production of hydroxyl radicals and consequently enhances the efficiency of photocatalytic degradation [12,30]. The effect of light enhancement by Ag is also confirmed in the UV–vis diffuse reflectance spectroscopy (DRS) analysis depicted in Fig. S5. The DR spectrum of Ag-ZnO shows a unique UV absorption band in the UV region of ZnO and SPR absorption property of Ag.

Finally, we performed FDTD simulations on a Ag NP with a diameter of 150 nm and a Ag-ZnO NP with a Ag core diameter of 150 nm and a ZnO shell thickness of d = 2.5–10 nm (Fig. 6) using the properties of Ag and the wavelength dependences of the ZnO refractive index and the ZnO absorption coefficient included in the FDTD solution library. A plane wave with a wavelength of either 382 or 633 nm was incident on the NP along the y-axis, and the enhancement factor was derived by dividing the monitored light intensity by that of the incident light around the NP. The polarization direction was along the z-axis. Fig. 7 (a)–(e) shows the distribution of light enhancement at 633 nm as a function of ZnO shell thickness, revealing that obvious light enhancement was observed near the NP surface, especially in the incident polarization (i.e., z-) direction. The light enhancement factor of the Ag-ZnO NP at 633 nm monotonously increased with increasing ZnO thickness, as highlighted by the concomitant extension of the enhancement area along the z-direction. This behavior agreed with the fact that the absorption coefficient of ZnO at this wavelength is negligibly small, which facilitates the observation of light enhancement effects.

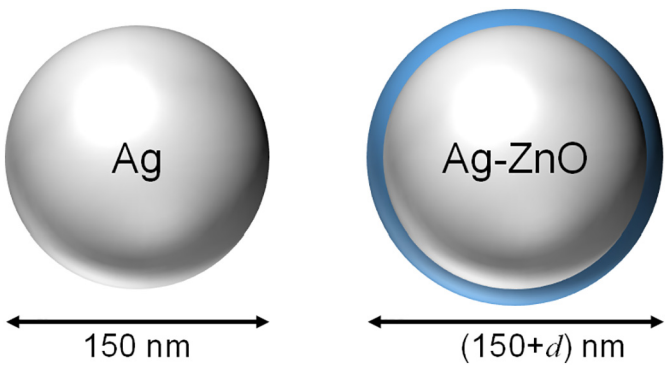

Fig. 6. Schematic cross-sections of Ag and Ag-ZnO NPs studied by FDTD simulation, with the thickness of the ZnO shell denoted as d.

Fig. 7(f)–(j) shows the distribution of light enhancement at 382 nm as a function of ZnO shell thickness, demonstrating that maximal enhancement was observed at a shell thickness of 2.5 nm. However, a substantial decrease of the enhancement factor was observed when the ZnO thickness increased beyond 7.5 nm. This behavior was ascribed to the fact that ZnO exhibits a characteristic UV absorbance due to its band gap. Therefore, light non-enhancement is observed when the thickness of ZnO is sufficiently large to offset the light enhancement effects of the core-shell structure.

4. Conclusions

Ag-ZnO NPs were successfully fabricated by rotational ALD. The Ag cores were uniformly coated with thin ZnO layers having a stable wurtzite structure. The photocatalytic activity of the Ag-ZnO NPs for RhB degradation under artificial sunlight irradiation (k = 0.0430 min^{-1}, >98% degradation of RhB within 100 min) was superior to those of ZnO and ZnO-ZnO NPs. The result was mainly ascribed to the efficient separation of e^{-}–h^{+} pairs, which was induced by Ag cores. The simulation also confirmed that the photocatalyst could show enhanced performance by thinly coating the semiconductor ZnO on Ag. Consequently, the fabrication of NPs with metal core-semiconductor shell architectures was concluded to hold great potential for the utilization of solar light to solve environmental problems.

Acknowledgements

This work was supported by the Basic Science Research Program (2012R1A6A1029029) through the National Research Foundation of Korea (NRF) funded by the Ministry of Education. This work was also supported by the Commercialization Promotion Agency for R&D Outcomes (COMPA) funded by the Ministry of Science and ICT (2019K000024).

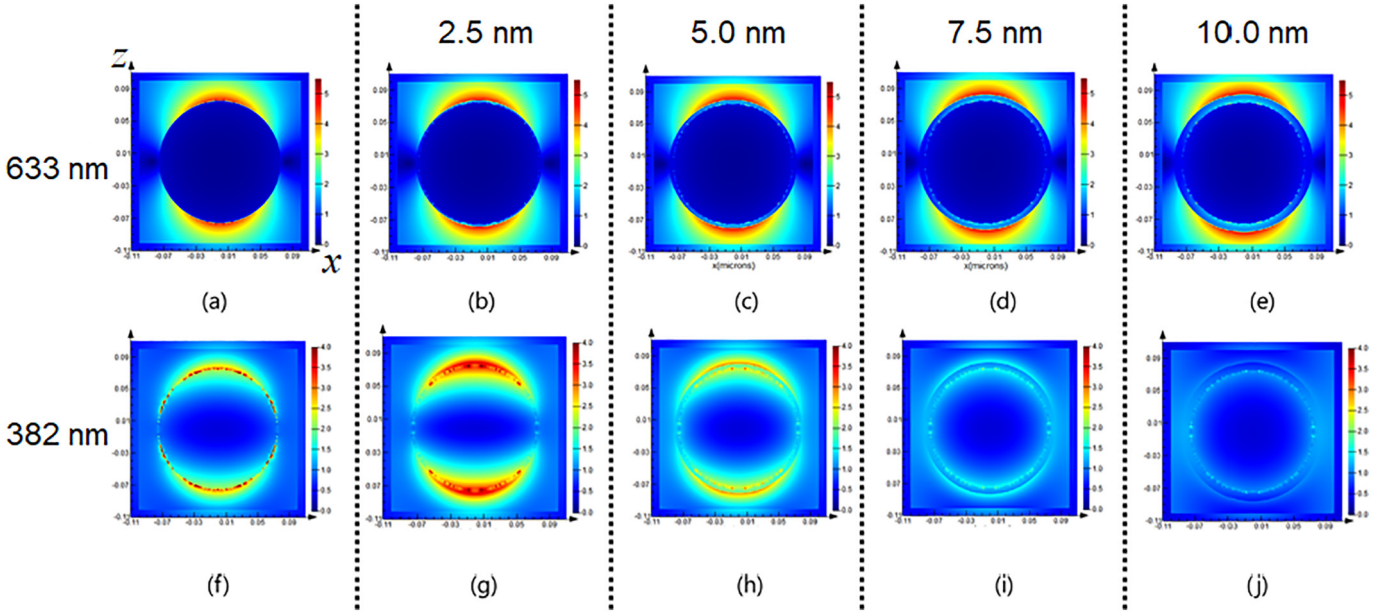

Fig. 7. Factors describing the enhancement of light intensity around a Ag-ZnO core-shell NP for wavelengths of 633 nm (a–e) and 382 nm (f–j). ZnO shell thickness was increased from (a, f) 0 nm to 10 nm (e, j) in steps of 2.5 nm.

Appendix A. Supplementary data

Supplementary data to this article can be found online at https://doi.org/10.1016/j.matdes.2019.107831.

References

[1] K.M. Lee, C.W. Lai, K.S. Ngai, J.C. Juan, Recent developments of zinc oxide based photocatalyst in water treatment technology: a review, Water Res. 88 (2016) 428–448.
[2] N. Zhang, S.Q. Liu, Y.J. Xu, Recent progress on metal core@semiconductor shell nanocomposites as a promising type of photocatalyst, Nanoscale 4 (7) (2012) 2227–2238.
[3] S. Seong, Y.C. Jung, T. Lee, I.S. Park, J. Ahn, Fabrication of Fe_3O_4-ZnO core-shell nanoparticles by rotational atomic layer deposition and their multi-functional properties, Curr. Appl. Phys. 16 (12) (2016) 1564–1570.
[4] S.H. Guo, X.H. Li, X.G. Ren, L. Yang, J.M. Zhu, B.Q. Wei, Optical and electrical enhancement of hydrogen evolution by MoS_2@MoO_3 core-shell nanowires with designed tunable plasmon resonance, Adv. Funct. Mater. 28 (32) (2018) 13.
[5] X.H. Zhao, S. Su, G.L. Wu, C.Z. Li, Z. Qin, X.D. Lou, J.G. Zhou, Facile synthesis of the flower-like ternary heterostructure of Ag/ZnO encapsulating carbon spheres with enhanced photocatalytic performance, Appl. Surf. Sci. 406 (2017) 254–264.
[6] D. Longrie, D. Deduytsche, C. Detavernier, Reactor concepts for atomic layer deposition on agitated particles: a review, J. Vac. Sci. Technol. A 32 (1) (2014) 13.
[7] P. Zhao, D.Y. Ma, Preparation and photocatalytic performance of SnO_2@TiO_2 core-shell nanowires, Rare Metal Mater. Eng. 46 (11) (2017) 3538–3543.
[8] X.R. Wang, G. Yushin, Chemical vapor deposition and atomic layer deposition for advanced lithium ion batteries and supercapacitors, Energy Environ. Sci. 8 (7) (2015) 1889–1904.
[9] K. Wenderich, G. Mul, Methods, mechanism, and applications of photodeposition in photocatalysis: a review, Chem. Rev. 116 (23) (2016) 14587–14619.
[10] S.K. Shrama, N. Saurakhiya, S. Barthwal, R. Kumar, A. Sharma, Tuning of structural, optical, and magnetic properties of ultrathin and thin ZnO nanowire arrays for nano device applications, Nanoscale Res. Lett. 9 (2014) 17.
[11] X.T. Chang, Z.L. Li, X.X. Zhai, S.B. Sun, D.X. Gu, L.H. Dong, Y.S. Yin, Y.Q. Zhu, Efficient synthesis of sunlight-driven ZnO-based heterogeneous photocatalysts, Mater. Des. 98 (2016) 324–332.
[12] J.Y. Xiong, Q. Sun, J. Chen, Z. Li, S.X. Dou, Ambient controlled synthesis of advanced core-shell plasmonic Ag@ZnO photocatalysts, Crystengcomm 18 (10) (2016) 1713–1722.
[13] M. Macias-Montero, R.J. Pelaez, V.J. Rico, Z. Saghi, P. Midgley, C.N. Afonso, A.R. Gonzalez-Elipe, A. Borras, Laser treatment of Ag@ZnO nanorods as long-life-span SERS surfaces, ACS Appl. Mater. Interfaces 7 (4) (2015) 2331–2339.
[14] X.H. Li, S.H. Guo, C.X. Kan, J.M. Zhu, T.T. Tong, S.L. Ke, W.C.H. Choy, B.Q. Wei, Au Multimer@MoS_2 hybrid structures for efficient photocatalytical hydrogen production via strongly plasmonic coupling effect, Nano Energy 30 (2016) 549–558.
[15] S.H. Guo, X.H. Li, J.M. Zhu, T.T. Tong, B.Q. Wei, Au NPs@MoS_2 sub-micrometer sphere-ZnO nanorod hybrid structures for efficient photocatalytic hydrogen evolution with excellent stability, Small 12 (41) (2016) 5692–5701.
[16] T.X. Liu, B.X. Li, Y.G. Hao, F. Han, L.L. Zhang, L.Y. Hu, A general method to diverse silver/mesoporous-metal-oxide nanocomposites with plasmon-enhanced photocatalytic activity, Appl. Catal. B Environ. 165 (2015) 378–388.
[17] T.T. Jiang, X.Y. Qin, Y. Sun, M. Yu, UV photocatalytic activity of Au@ZnO core-shell nanostructure with enhanced UV emission, RSC Adv. 5 (80) (2015) 65595–65599.
[18] L. Paussa, L. Guzman, E. Marin, N. Isomaki, L. Fedrizzi, Protection of silver surfaces against tarnishing by means of alumina/titania-nanolayers, Surf. Coat. Technol. 206 (5) (2011) 976–980.
[19] R.S. Patil, M.R. Kokate, D.V. Shinde, S.S. Kolekar, S.H. Han, Synthesis and enhancement of photocatalytic activities of ZnO by silver nanoparticles, Spectrochim. Acta A Mol. Biomol. Spectrosc. 122 (2014) 113–117.
[20] R.L. Puurunen, W. Vandervorst, Island growth as a growth mode in atomic layer deposition: a phenomenological model, J. Appl. Phys. 96 (12) (2004) 7686–7695.
[21] W. Zhang, G. Wang, Z.Y. He, C.Y. Hou, Q.H. Zhang, H.Z. Wang, Y.G. Li, Ultralong ZnO/Pt hierarchical structures for continuous-flow catalytic reactions, Mater. Des. 109 (2016) 492–502.
[22] M.D.L. Balela, C.M.O. Pelicano, J.D. Ty, H. Yanagi, Formation of zinc oxide nanostructures by wet oxidation of vacuum deposited Zn thin film, Opt. Quant. Electron. 49 (1) (2017) 11.
[23] M.G. Nair, M. Nirmala, K. Rekha, A. Anukaliani, Structural, optical, photo catalytic and antibacterial activity of ZnO and Co doped ZnO nanoparticles, Mater. Lett. 65 (12) (2011) 1797–1800.
[24] S. Yamabi, H. Imai, Growth conditions for wurtzite zinc oxide films in aqueous solutions, J. Mater. Chem. 12 (12) (2002) 3773–3778.
[25] G.J. Soldano, F.M. Zanotto, M.M. Mariscal, Mechanical stability of zinc oxide nanowires under tensile loading: is wurtzite stable at the nanoscale? RSC Adv. 5 (54) (2015) 43563–43570.
[26] H. Razavi-Khosroshahi, K. Edalati, J. Wu, Y. Nakashima, M. Arita, Y. Ikoma, M. Sadakiyo, Y. Inagaki, A. Staykov, M. Yamauchi, Z. Horita, M. Fuji, High-pressure zinc oxide phase as visible-light-active photocatalyst with narrow band gap, J. Mater. Chem. A 5 (38) (2017) 20298–20303.
[27] Y. Chen, L.N. Zhang, L.C. Ning, C.J. Zhang, H. Zhao, B. Liu, H.Q. Yang, Superior photocatalytic activity of porous wurtzite ZnO nanosheets with exposed {001} facets and a charge separation model between polar (001) and (00(1)over-bar) surfaces, Chem. Eng. J. 264 (2015) 557–564.
[28] P.S. Venkatesh, V. Purushothaman, S.E. Muthu, S. Arumugam, V. Ramakrishnan, K. Jeganathan, K. Ramamurthi, Role of point defects on the enhancement of room temperature ferromagnetism in ZnO nanorods, CrystEngComm 14 (14) (2012) 4713–4718.
[29] W.D. Oh, Z.L. Dong, T.T. Lim, Generation of sulfate radical through heterogeneous catalysis for organic contaminants removal: current development, challenges and prospects, Appl. Catal. B-Environ. 194 (2016) 169–201.
[30] K. Mondal, A. Sharma, Recent advances in the synthesis and application of photocatalytic metal-metal oxide core-shell nanoparticles for environmental remediation and their recycling process, RSC Adv. 6 (87) (2016) 83589–83612.